ADSORPTION PROPERTIES OF ZSM-5 ZEOLITES*

Pavol HUDEC[a1], Agata SMIESKOVA[a2], Zdenek ZIDEK[a3], Milan ZUBEK[b], Petr SCHNEIDER[c], Milan KOCIRIK[d] and Jana KOZANKOVA[e]

[a] *Department of Petroleum Technology and Petrochemistry, Slovak University of Technology, 812 37 Bratislava, Slovak Republic; e-mail:* [1] *phudec@chelin.chtf.stuba.sk,*
[2] *smiesko@chelin.chtf.stuba.sk,* [3] *zidek@checdek.chtf.stuba.sk*
[b] *Research Institute for Petroleum and Hydrocarbon Gases, 824 12 Bratislava, Slovak Republic; e-mail: zubek@slovnaft.sk*
[c] *Institute of Chemical Process Fundamentals, Academy of Sciences of the Czech Republic, 165 02 Prague 6-Suchdol, Czech Republic; e-mail: schneider@icpf.cas.cz*
[d] *J. Heyrovsky Institute of Physical Chemistry, Academy of Sciences of the Czech Republic, 182 23 Prague 8, Czech Republic; e-mail: milan.kocirik@jh-inst.cas.cz*
[e] *Department of Ceramics, Glass and Cement, Slovak University of Technology, 81 237 Bratislava, Slovak Republic; e-mail: kozanko@chelin.chtf.stuba.sk*

Received February 11, 1997
Accepted July 23, 1997

Adsorption properties determined by physical adsorption of nitrogen for a series of ZSM-5 zeolite samples with various Si/Al ratios and different crystal size were compared. In addition to the BET method, the *t*-plot method was used to determine the microporosity of samples. Very small crystals of ZSM-5 zeolites, generally below 1 μm, with Si/Al ratio between 14 and 21 exhibit adsorption isotherms typical for purely microporous solids. Samples with Si/Al ratios larger than (about) 95 show low-pressure steps and hysteresis loops and, depending on crystal morphology, also high-pressure hysteresis loops. The low-pressure steps were associated with steps on *t*-plots which showed two linear parts. Small increase of adsorption up to relative pressure 0.2 is characteristic for samples with Si/Al ratios between 25 and 50.

Key words: ZSM-5 zeolites; Adsorption; *t*-Plot; Crystal size and morphology; Microporosity.

ZSM-5 zeolites are most frequently used in the preparation of selective catalysts for a variety of reactions in petrochemistry and organic technology[1,2]. Their unique properties follow from the specific structure of the pore system which consists of pores with 0.51–0.55 nm diameter.

While the first synthesis of a ZSM-5 zeolite was carried out in the presence of a tetraalkylammonium cation as a template[3], it is possible to prepare ZSM-5 zeolites in the presence of a large number of organic compounds[4,5] or even in the absence of

* Presented at the Symposium on Diffusion in Zeolites and Other Microporous Materials at the 12th CHISA'96 Congress, Prague, August 25–30, 1996.

organic templates[6]. The character of template, as well as the Si/Al ratio in the starting gel and conditions of crystallization determine the morphology and size of crystals and, consequently, also sorption and catalytic properties.

The most important characteristics of ZSM-5 crystals follow from the analysis of data on physical adsorption of nitrogen. While the BET isotherm supplies meaningless values of specific surface, because the adsorption in micropores proceeds *via* pore-volume filling and not by multilayer adsorption, the use of α-plot[7] and *t*-plot[7,8] methods, or combination of BET and Dubinin isotherms[9], gives the possibility to separate the volume of micropores from external and mesopore surface.

In this work, the correlations were studied between the mode of synthesis and structure of ZSM-5 type zeolites on the one hand, and the adsorption properties of nitrogen evaluated by BET isotherm and *t*-plot method on the other.

EXPERIMENTAL

ZSM-5 samples, prepared in the presence of various types of templates with Si/Al ratio from 14 up to pure silicate, were studied (Table I).

Scanning electron microscopy (SEM) with JXA-840A (JEOL) equipment was used for crystal size and morphology determinations.

Physical adsorption of nitrogen at the normal boiling point of liquid nitrogen was performed on Sorptomatic 1800, Sorptomatic 1900 (Carlo Erba), DigiSorb 2600 and ASAP 2000 (Micromeritics) volumetric instruments. Before measurement, samples were evacuated overnight at 670 K and 0.1 Pa.

TABLE I
Characteristics of ZSM-5 samples

Sample No.	Synthesis template	Si/Al	Crystal size, μm
1	TPA-Br	14	<0.1
2	TPA-Br	21	0.1
3[a]	EtOH + Na_2HPO_4	22.5	0.2–6
4	TPA-OH	31	20 × 10 × 10
5	TPA-Br	48	0.5–3
6	TPA-Br	98	2.5
7	TPA-Br	600	4–4.5
8[b]	TPA-Br + TPA + $Ti(OR)_4$	935	2.7 × 1.8 × 0.4
9[c]	TPA-Br	∞	200 × 40 × 40
10[d]	i-PrOH + NH_4OH	14[e]	1–3

All samples, excepting 3 and 9, were prepared in the Research Institute for Petroleum and Hydrocarbon Gases, Bratislava. TPA-Br, TPA-OH tetrapropylammonium bromide and hydroxide, respectively; EtOH ethanol; i-PrOH isopropyl alcohol; $Ti(OR)_4$ tetraethyl orthotitanate.
[a] Supplied by Prof. Mostowicz, Poland. [b] Sample contains 2.29 wt.% of TiO_2, Si/(Al + Ti) = 28. [c] Prepared in the J. Heyrovsky Institute of Physical Chemistry, Academy of Sciences of the Czech Republic, Prague. [d] Prepared by deep-bed treatment of the ammonium form of ZSM-5 zeolite at 1 050 K for 3 h. [e] In the bulk.

Data Analysis

Specific surface area S_{BET} was determined by the BET isotherm method in the range of P/P_0 = 0.05–0.3.

Micropore volumes were determined by the application the *t*-plot method[8] to nitrogen adsorption data. According to this method, the volume of nitrogen adsorbed is plotted against *t* (thickness of nitrogen layer) for the nitrogen on a non-porous reference solid (standard isotherm). For non-microporous solids, the linearization of *t*-plot in the range of free multilayer adsorption (obviously for *t* = 0.35–0.6 nm, corresponding to P/P_0 about 0.08–0.45) leads to zero intercept on V_a-axis. The external surface area can be obtained from the slope of the *t*-plot, the value for non-microporous solids should be equal to the S_{BET}. For microporous solids, the intercept on V_a-axis gives the volume of micropores V_{micro}, from slope of the *t*-plot the specific surface of mesopores and external surface S_t is calculated.

As standard isotherm, the equation of de Boer[10] derived by fitting the master isotherm to the Harkins and Jura adsorption equation[11] was used:

$$t = 0.1\ (13.99/\log (P_0/P) + 0.034)^{1/2}\ , \qquad (1)$$

where *t* (in nm) is the statistical thickness of adsorbed layer of nitrogen, 13.99 and 0.034 are experimentally derived parameters for alumina-based non-porous material.

The application of the *t*-plot for the evaluation of zeolites is documented in Fig. 1. For zeolites with narrow to wide pore sizes (KNa-erionite, Na-mordenite and NaY-type) as well as for USY-zeolite with secondary mesopore structure, documented by hysteresis loop on adsorption isotherm, the *t*-plots are perfectly linear in the *t*-range 0.35–1 nm (P/P_0 = 0.08–0.75). This demonstrates multilayer adsorption on external surface of zeolite crystals.

Pore size distributions were determined from desorption branches of isotherms.

RESULTS AND DISCUSSION

The main characteristics of tested samples of ZSM-5 zeolites are summarized in Table I, morphology of crystals is shown in Figs 2–11. As can be seen, the Si/Al ratio increases from 14 for sample 1 to infinity for silicalite – sample 9; at the same time, a general increase in crystal size is apparent. While samples with Si/Al in the interval 14–21 have crystal sizes much less than 1 μm, the size of silicalite crystals is 200 μm. On the other

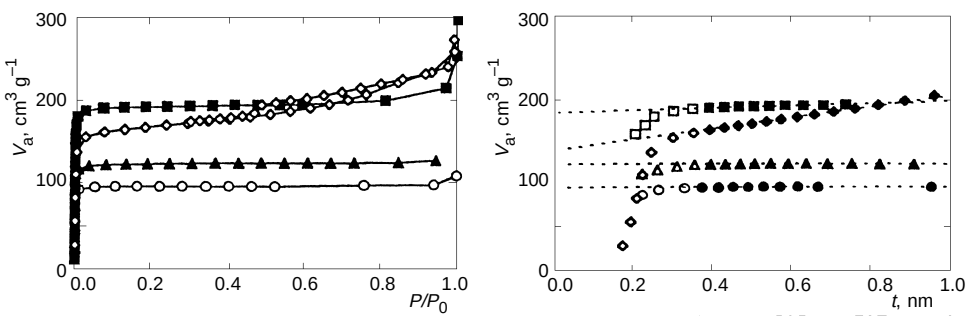

FIG. 1
Adsorption isotherms and *t*-plots of KNa-erionite (▲), Na-mordenite (❍), NaY (■) and USY (✧)

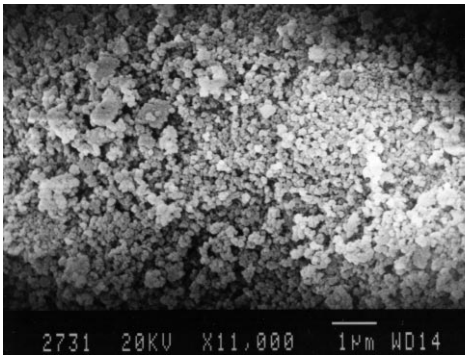

FIG. 2
SEM image of sample 1

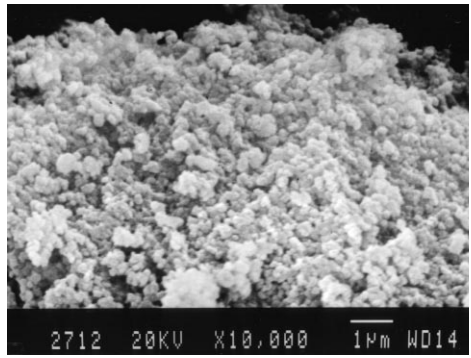

FIG. 3
SEM image of sample 2

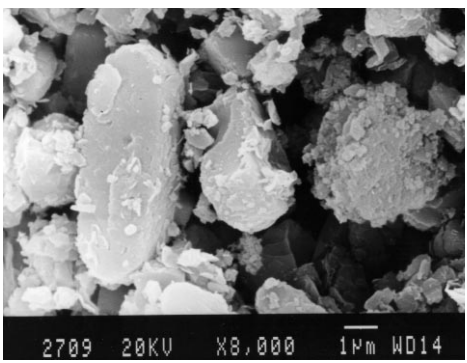

FIG. 4
SEM image of sample 3

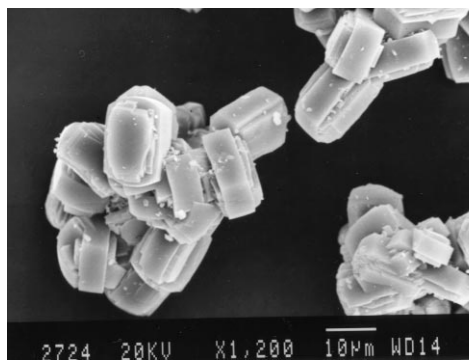

FIG. 5
SEM image of sample 4

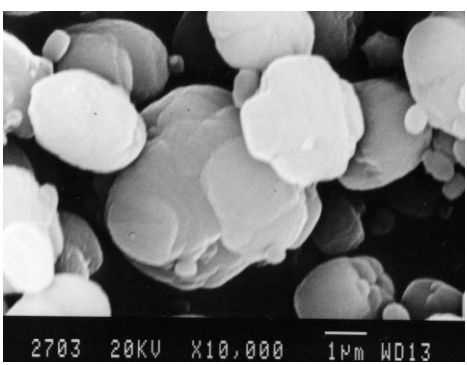

FIG. 6
SEM image of sample 5

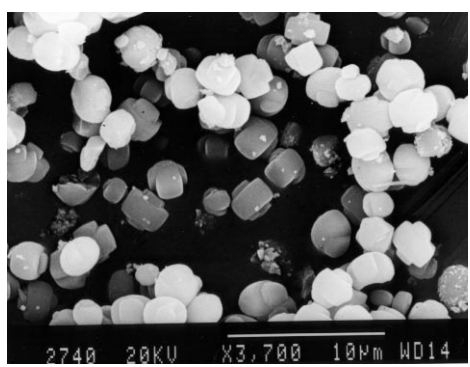

FIG. 7
SEM image of sample 6

hand, sample 3, synthesized in the presence of ethanol as template, has much larger crystals than sample 2, with nearly the same Si/Al ratio, and larger than samples 5–8 with much higher Si/Al ratio. Also, morphology of crystals is quite different and depends on the synthesis template and Si/Al ratio. Silicate (sample 9) was prepared in the form of large, well shaped separate crystals, while the form of crystals of samples 1 and 2, which occur in aggregates, is not easily detectable. Samples 5–7, synthesized under similar conditions, have similar morphology of twinned crystals the size of which increases with the Si/Al ratio. From Figs 6–8 it is clear that with the increase in the Si/Al ratio, the distribution of crystal sizes becomes more uniform. Samples 3 and 10, synthesized in the presence of alcohols, are of prismatic shape and their size increases with the Si/Al ratio. Sample 8, prepared in the presence of a Ti compound, has well formed plate crystals of orthorhombic shape.

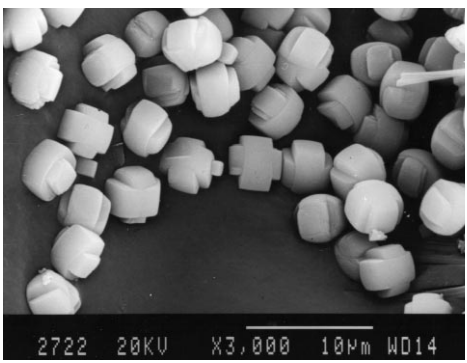

FIG. 8
SEM image of sample 7

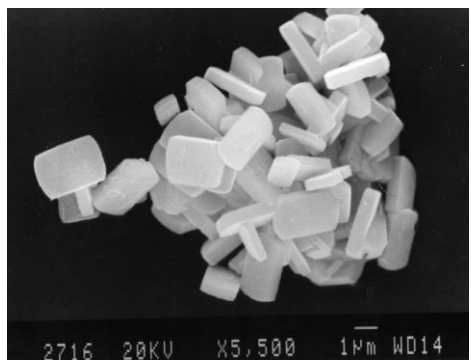

FIG. 9
SEM image of sample 8

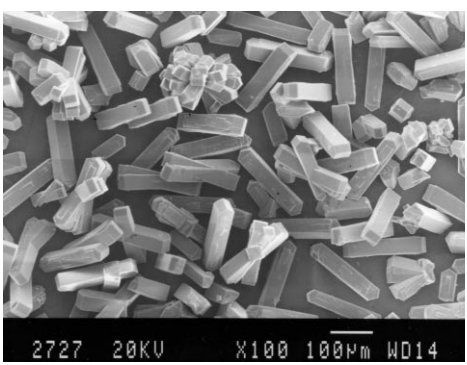

FIG. 10
SEM image of sample 9

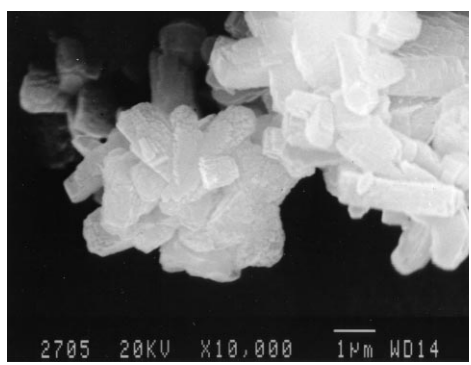

FIG. 11
SEM image of sample 10

Adsorption isotherms and *t*-plots are shown in Figs 12–21. The sorption characteristics (BET specific surface, S_{BET}, volume of micropores, V_{micro}, specific external surface plus surface of mesopores, S_t) are summarized in Table II.

Samples 1–3 have quite low Si/Al ratios and adsorption isotherms showing only volume filling of micropores and no presence of mesopores. Samples 1 and 2 exhibit isotherms typical for adsorption in primary micropores[12] (adsorption completed at $P/P_0 = 0.01$) with further nitrogen consumption due to adsorption on external crystal surface. For both samples, the *t*-plots show good linearity in the *t*-range 0.35–0.8 nm. The adsorption contribution due to the external surface is corroborated by the S_t values; for small crystals of sample 1, $S_t = 90.8$ m^2 g^{-1}, *i.e.*, twice the value for larger crystals 2, ($S_t = 46$ m^2 g^{-1}). The small hysteresis loop at $P/P_0 > 0.9$ can be ascribed to the interparticle voids among very fine crystals; *cf.* Figs 2 and 3.

On the other hand, sample 9 (silicalite with large crystals, Fig. 20) shows a low-pressure hysteresis loop at $P/P_0 = 0.1$–0.2 and very little additional adsorption up to high relative pressures. The low-pressure hysteresis loop is also observed for sample 6 and 7 (Figs 17 and 18) with Si/Al of 98 and 600. A narrow low-pressure hysteresis loop together with a high-pressure hysteresis loop, which corresponds to the secondary

TABLE II
Sorption characteristics of ZSM-5 samples by the BET and *t*-plot methods

Sample No.	S_{BET}, m^2 g^{-1}	*t*-Range, nm	V_{micro}, cm^3 g^{-1}	S_t, m^2 g^{-1}
1	323	0.35–0.8	0.124	90.8
2	313	0.35–0.8	0.138	45.9
3	268	0.35–0.7	0.116	36.2
4	352	0.32–0.46	0.090	
		0.47–0.9	0.177	22.7
5	366	0.31–0.45	0.125	
		0.45–0.8	0.165	46.7
6	352	0.25–0.41	0.118	
		0.55–1.0	0.171	11.6
7	321	0.29–0.38	0.111	
		0.55–1.2	0.152	13.3
8	333	0.36–0.52	0.131	
		0.52–0.9	0.159	19.7
9	383	0.23–0.39	0.134	
		0.5–1.3	0.185	2.16
10	338	0.23–0.38	0.111	
		0.50–1.0	0.149	40.1

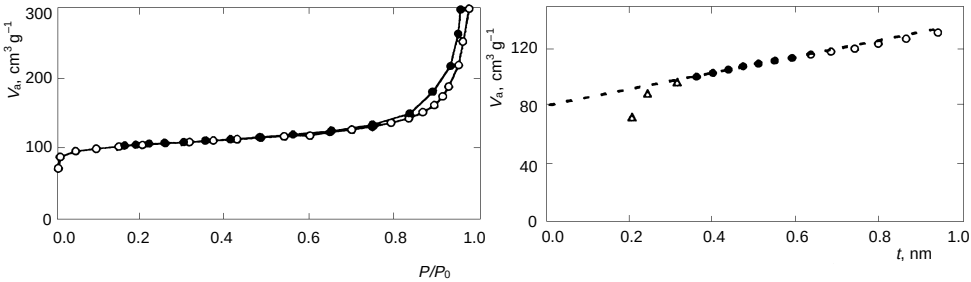

FIG. 12
Adsorption isotherm (❍ adsorption, ● desorption) and *t*-plot (● linearized part, Δ lower and ❍ upper nonlinearized parts) of sample 1

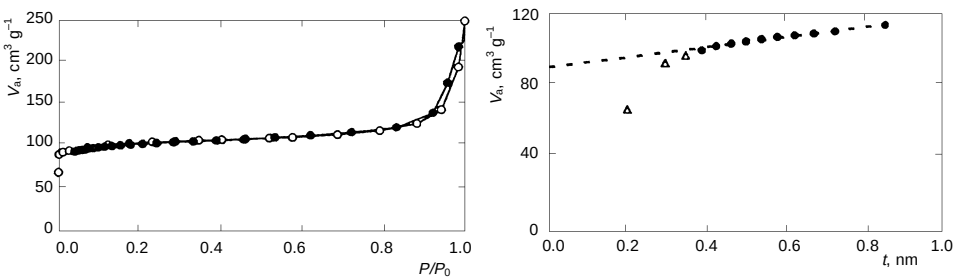

FIG. 13
Adsorption isotherm (❍ adsorption, ● desorption) and *t*-plot (● linearized part, Δ lower nonlinearized part) of sample 2

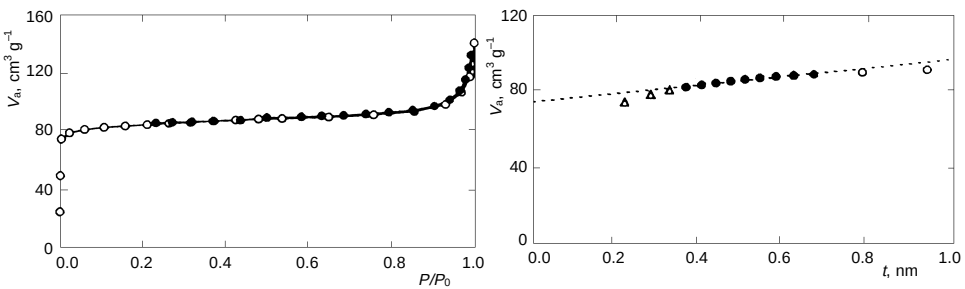

FIG. 14
Adsorption isotherm (❍ adsorption, ● desorption) and *t*-plot (● linearized part, Δ lower and ❍ upper nonlinearized parts) of sample 3

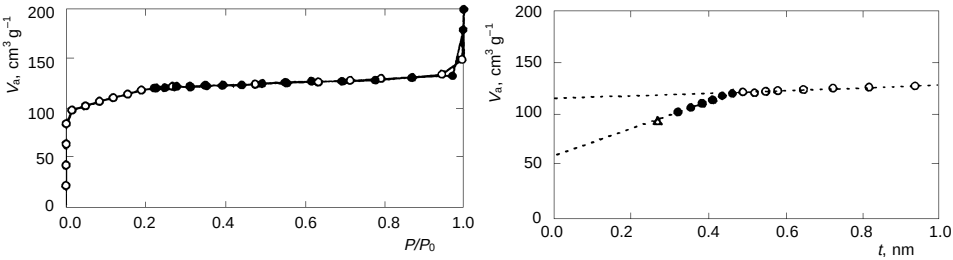

FIG. 15

Adsorption isotherm (❍ adsorption, ● desorption) and *t*-plot (Δ nonlinearized part, ●lower and ❍ upper linearized parts) of sample 4

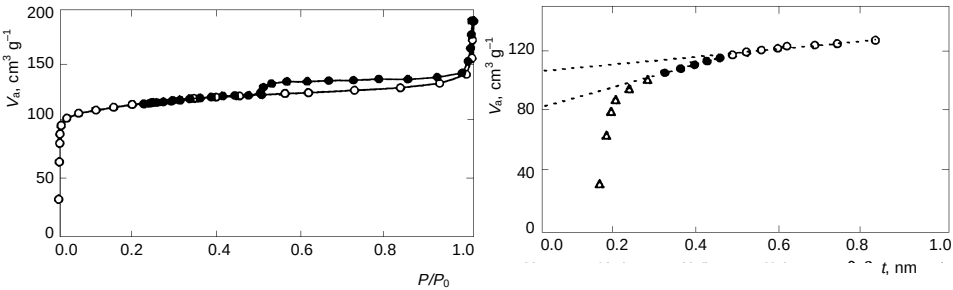

FIG. 16

Adsorption isotherm (❍ adsorption, ● desorption) and *t*-plot (Δ nonlinearized part, ●lower and ❍ upper linearized parts) of sample 5

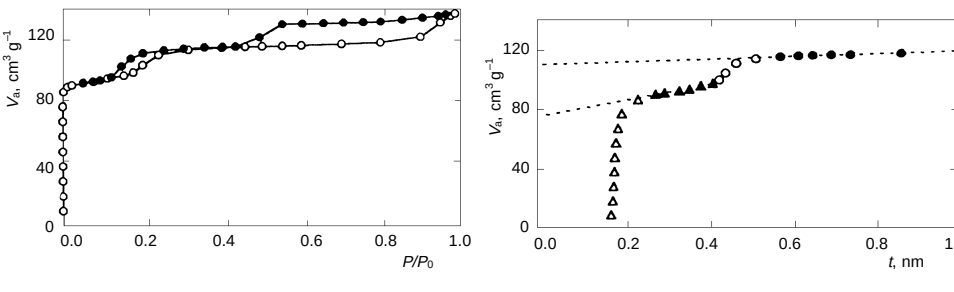

FIG. 17

Adsorption isotherm (❍ adsorption, ● desorption) and *t*-plot (Δ, ❍ nonlinearized parts, ▲ lower and ● upper linearized parts) of sample 6

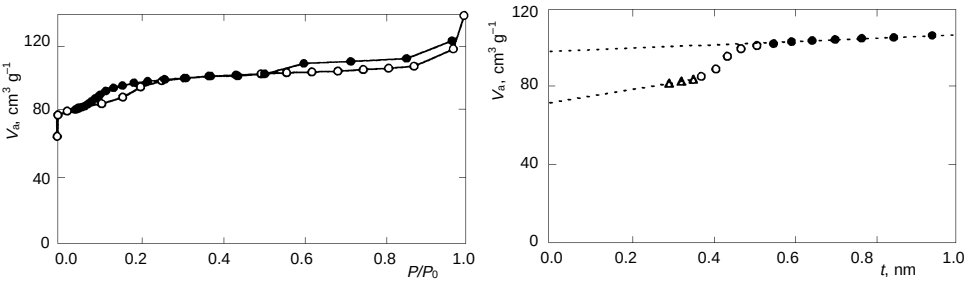

FIG. 18
Adsorption isotherm (❍ adsorption, ● desorption) and *t*-plot (❍ nonlinearized part, Δ lower and ● upper linearized parts) of sample 7

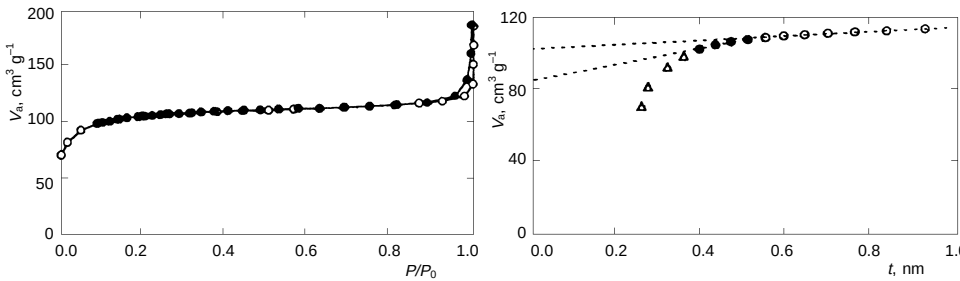

FIG. 19
Adsorption isotherm (❍ adsorption, ● desorption) and *t*-plot (Δ, ❍ nonlinearized parts, ●lower and ❍ upper linearized parts) of sample 8

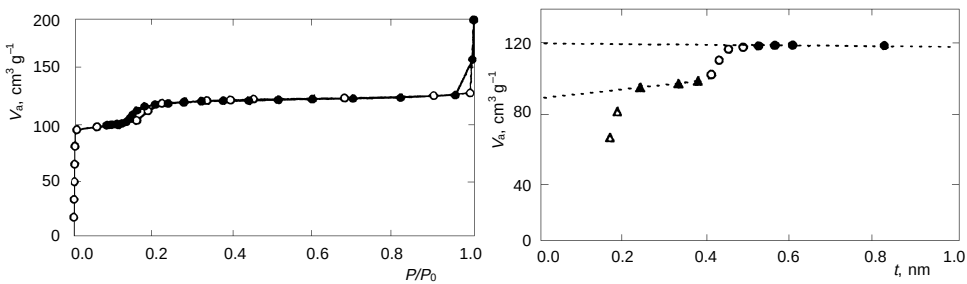

FIG. 20
Adsorption isotherm (❍ adsorption, ● desorption) and *t*-plot (Δ, ❍ nonlinearized parts, ▲ lower and ● upper linearized parts) of sample 9

mesoporous structure, appears also for sample 10, dealuminated by the treatment under deep-bed conditions (Fig. 21).

The low-pressure hysteresis loops were already reported by several authors for ZSM-5 zeolites with Si/Al larger than 45–70 and for silicalite[13–15]. The sharpness of the low-pressure hysteresis loop increases with the Si/Al ratio. Various explanations for this phenomenon were proposed. The *in situ* neutron diffraction measurements of the system

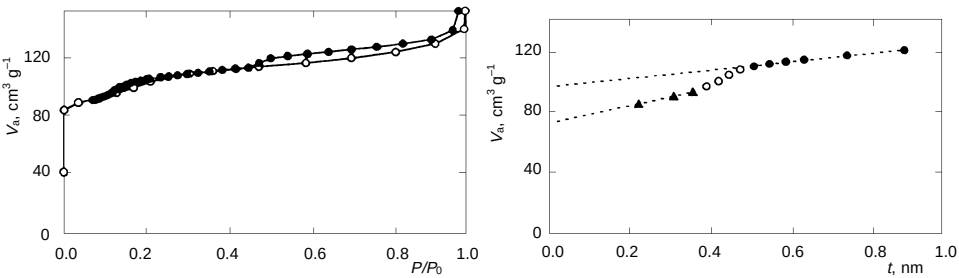

FIG. 21
Adsorption isotherm (❍ adsorption, ● desorption) and *t*-plot (❍ nonlinearized part, ▲ lower and ● upper linearized parts) of sample 10

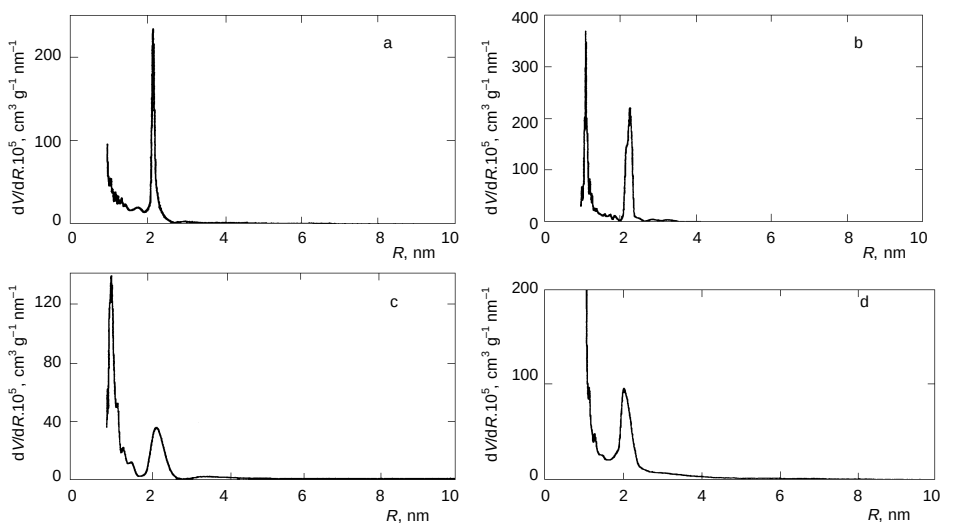

FIG. 22
Pore size distribution of samples 5 (a), 6 (b), 7 (c) and 10 (d)

silicalite/nitrogen at 77 K detected changes of both ZSM-5 (monoclinic–orthorhombic) and nitrogen (liquid–solid) structure with increasing adsorbate coverage[16]. A model based on interaction of admolecules was suggested for explanation of low-pressure hysteresis loops[17]. Generally, the low-pressure step and hysteresis loops were observed only for high-silica ZSM-5 structures using nitrogen as adsorbate, and for samples of ZSM-5 zeolites dealuminates by HCl or steaming[18]. This phenomenon was observed neither on silicalite/argon[14] nor on ZSM-11 with pore structure very similar to ZSM-5 zeolite[19] with the same Si/Al ratio.

Analysis of adsorption isotherms with low-pressure hysteresis loops by the *t*-plot method shows two linear parts. The upper part starts at t = 0.5–0.55 nm and represents adsorption of nitrogen on external surface of zeolite crystals (sample 9) and in mesopores (samples 6, 7 and 10). *t*-Plots of samples with low-pressure hysteresis loop (Figs 17, 18, 20, and 21) exhibit a lower linear part in *t*-range from 0.23–0.29 nm to 0.38–0.41 nm. The ratios of volumes of micropores, V_{micro}, obtained from intercepts of both linear parts of *t*-plots are in the range 1.35–1.45, *i.e.*, nearly the same as the reported ratio of volumes of nitrogen adsorbed in the solid phase (30.5 molecules/unit cage) and liquid phase (22 molecules/unit cage)[20].

Interesting is the nitrogen physical adsorption on sample 8 with a high Si/Al ratio (Si/Al = 935) containing 2.3 wt.% of titanium oxide (Fig. 19). In this low-aluminum sample with well formed crystals, the low-pressure hysteresis loop is not present as expected for such a high Si/Al ratio. Adsorption isotherm shows quite a high adsorption in the range $P/P_0 < 0.2$ which is reflected also by the *t*-plot curvature in the *t*-range below 0.5 nm. Similar isotherms and *t*-plots are observed also with samples 4 and 5 and partially also for sample 3. All these samples have the Si/Al ratios between 23 and 48, *i.e.*, between the low silica samples with ideal zeolitic isotherm (samples 1 and 2, Figs 12 and 13) and high-silica samples with low-pressure hysteresis loops. It was already shown that the low-pressure hysteresis loops are controlled by adsorption equilibrium and not by the kinetic effect[16] and that they appear in samples with the Si/Al ratios higher than about 50 (refs[13–15]). It seems that with sample 8, where the ratio of Si/(Al + Ti) = 28, the titania in the crystal structure of zeolite has similar influence on sorption properties as aluminum.

By summarizing the obtained results of nitrogen adsorption, it is possible to classify the ZSM-5 samples according to the types of adsorption isotherms into three basic groups:

Type **A** has an adsorption isotherm of the Lamgmuir type up to high relative pressures. The corresponding linear part of the *t*-plot spans the *t*-range from 0.35 to 0.6 or even higher. To this type, the high-aluminum samples 1 and 2 belong.

Type **B** exhibits increased adsorption at $P/P_0 < 0.2$. This is reflected by curved *t*-plots in the *t*-range 0.35–0.6, where the second layer of adsorbed nitrogen is formed. This

type is represented by samples 4 and 5 with Si/Al 31 and 48, and by titanium-containing sample 8.

Type **C** for high-silica samples. The isotherms contain low-pressure hysteresis loops in the range of $0.1 < P/P_0 < 0.2$. The *t*-plots contain two linear regions, as can be seen for samples 6, 7 and 9.

On isotherms of types **B** and **C** a high-pressure hysteresis loop resulting from the capillary condensation in mesopores, appears.

The group of samples 4 (Si/Al = 31), 5 (Si/Al = 48) and 8 (Si/(Al + Ti) = 28), Figs 15, 16 and 19, is located between the group of low-silica samples 1 and 2, with simple Langmuir adsorption isotherms, Figs 12 and 13, and the group of high-silica samples 6, 7, 9 and 10, with low-pressure hysteresis loops, Figs 17, 18, 20 and 21.

The question is, if the non-linearity of *t*-plots of type **B** samples could be ascribed to the intermediate Si/Al ratio. In this case only the Si/Al framework ratio should be responsible for the adsorption in the range of relative pressure 0.01–0.2 and for the corresponding deviation of *t*-plots from linearity. Such explanation could be based on changes in the interaction between adsorbed molecules of nitrogen and internal surface of zeolitic pores, depending on the Al content in the framework of the zeolite.

Nitrogen adsorption in the range of relative pressures 0.01–0.2 for samples 4 and 5 with Si/Al = 30–60 can be explained by quasi-multilayer adsorption in secondary micropores (supermicropores)[12]. This is, for instance, the case of samples 4 and 8, for which no mesopores appear on the pore-size distributions. The intercept of the extrapolated lower linear part of the *t*-plot for sample 4 (0.09 $cm^3\,g^{-1}$) reflects the real volume of primary micropores, and the difference between intercepts of extrapolated upper (0.177 $cm^3\,g^{-1}$) and lower (0.09 $cm^3\,g^{-1}$) linear parts of the *t*-plot can be ascribed to the secondary micropores.

The secondary mesopores could originate in the defects of zeolite crystals after synthesis or after thermal decomposition of the organic template. It is, however, not clear what is the source of mesopores in samples 5–7 with quite regular twinned crystals. As these samples were calcined before adsorption measurements only, the explanation of the mesopore presence must be the thermal treatment.

For samples 5–7, the pore size distributions show the same pore size of mesopores (R = 2.1–2.2 nm) as in sample 10 (see Fig. 22), where the secondary mesoporous system was created as a result of deep-bed treatment of the ammonium form of ZSM-5 sample. The lower maximum on pore-size distribution curves (R about 1 nm) for samples 6 and 7 has no physical meaning; it reflects the decrease on the low-pressure hysteresis loop.

CONCLUSIONS

Three basic types of nitrogen adsorption isotherms were observed in the investigated series of ZSM-5 zeolite samples.

A typical Langmuir form of adsorption isotherms was observed only for ZSM-5 zeolites with small Si/Al ratios, from 14 to 21, and very fine crystals (smaller than 1 μm). For those samples, the *t*-plot is linear from $t = 0.35$ to 0.6 nm and even higher, up to 1 nm.

High-silica samples of ZSM-5 with Si/Al above 90 show low-pressure hysteresis loops in the range of $P/P_0 = 0.1–0.2$, resulting also in the formation of the step and two linear parts on *t*-plot. The upper linear part corresponds to multilayer adsorption on external surface and in mesopores, while the micropore volume could correspond to solid nitrogen in micropores.

ZSM-5 samples with intermediate Si/Al ratios, 25–50, exhibit an increased adsorption at $P/P_0 < 0.2$, reflected by curved *t*-plots in the *t*-range 0.35–0.6 nm, where a second layer of adsorbed nitrogen is formed.

SYMBOLS

P/P_0	relative pressure
R	pore radius, nm
S_{BET}	specific surface area by the BET-isotherm method, $m^2\ g^{-1}$
S_t	specific surface area of external surface and mesopores by the *t*-plot, $m^2\ g^{-1}$
t	statistical thickness of adsorbed layer of nitrogen, nm
V_{micro}	specific volume of micropores by the *t*-plot, $cm^3\ g^{-1}$
V_a	adsorbed volume of gaseous nitrogen at STP, $cm^3\ g^{-1}$

This work was partially supported by the Grant Agency of the Czech Republic (Grant No. 203/96/0210). Adsorption measurements with Sorptomatic 1900 were supported by Tempus Jep-1125 Chemical Reaction Engineering.

REFERENCES

1. Chen N. Y., Garwood W. E.: *Catal. Rev.-Sci. Eng.* **1986**, *28*, 185.
2. Feast S., Lercher J. A.: *Stud. Surf. Sci., Catal.* **1996**, *102*, 363.
3. Argauer R. J., Landolt G. R.: U.S. 3 702 886 (1972).
4. Moretti E., Contessa S., Padovan M.: *Chim. Ind.* **1985**, *67*, 21.
5. Wilkosz J., Stobiecka E., Dudek B.: *Cryst. Res. Technol.* **1989**, *24*, 1129.
6. Dai F. Y., Suzuki M., Takahashi H., Saito Y.: *ACS Symp. Ser.* **1989**, *389*, 244.
7. Sing K. S. W., Everett D. H., Haul R. A. W., Moscou L., Pierotti R. A., Rouquerol J., Siemieniewska T.: *Pure Appl. Chem.* **1985**, *57*, 603.
8. Hudec P., Novansky J., Silhar S., Trung T., Zubek M., Madar J.: *Adsorpt. Sci. Technol.* **1986**, *3*, 159.
9. Remy M. J., Poncelet G.: *J. Phys. Chem.* **1995**, *99*, 773.
10. de Boer J. H., Lippens B. C., Linsen B. G., Broekhoff J. C. P., van den Heuvel A., Osinga Th. V.: *J. Colloid Interface Sci.* **1966**, *21*, 405.
11. Harkins W. D., Jura G.: *J. Am. Chem. Soc.* **1944**, *66*, 1366.
12. Carrot P. J. M., Sing K. S. W.: *Characterization of Porous Solids*, p. 77. Elsevier, Amsterdam 1988.
13. Handreck G. P., Smith T. D.: *J. Chem. Soc., Faraday Trans. 1* **1989**, *85*, 645.

14. Muller U., Unger K. K.: Ref.[12], p. 101.
15. Webb S. W., Conner W. C.: *Characterization of Porous Solids,* Vol. II, p. 31. Elsevier, Amsterdam 1991.
16. Reichert H., Muller U., Unger K. K., Grillet Y., Rouquerol F., Rouquerol J., Coulomb J. P.: Ref.[15], p. 535.
17. Pan D., Mersmann A.: *Zeolites* **1990**, *10*, 210.
18. Kornatowski J., Rozwadowski M., Lutz W., Baur W. H.: *Zeolites: A Refined Tool for Designing Catalytic Sites*, p. 259. Elsevier, Amsterdam 1995.
19. Hathaway P. E., Davis M. E.: *Catal. Lett.* **1990**, *5*, 333.
20. Muller U., Reichert H., Robens E., Unger K. K., Grillet Y., Rouquerol F., Rouquerol J., Pan D., Mersmann A.: *Fresenius Z. Anal. Chem.* **1989**, *333*, 433.